JOURNAL OF PROPULSION AND POWER
Vol. 16, No. 1, January–February 2000

Three-Dimensional Flow Analysis of Turbine Blade Cascades with Leading-Edge Ejection

Dieter Bohn,* Volker Becker,† and Karsten Kusterer†
Aachen University of Technology, D-52056 Aachen, Germany
and
Leonhard Fottner‡ and Sabine Ardey§
University of the Armed Forces Munich, D-85577 Neubiberg, Germany

The results of two different cooling configurations in a turbine cascade, one with slot ejection and one with shower-head ejection, are presented. Experimental and numerical results of the pressure distribution and the three-dimensional flowfield are compared. The numerical results correspond well with the experimental data. The investigations are performed for film-cooled cases with a blowing ratio of $M = 1.1$. It can be shown that complete discretization of the cooling channels and the plenum is necessary to obtain good aerodynamic results of the main flow because the complex flow structure in the ejection channels and the plenum has a significant influence on the calculated aerodynamic behavior of the blades. In the leading-edge area, the interaction of the cooling fluid jets and the main flow leads to mixture vortices and flow separations. Furthermore, the influence of secondary flow phenomena on the distribution of the cooling fluid along the blade surface is presented. On the suction side, the passage vortex leads to a displacement of cooling fluid in the direction of the midspan.

Nomenclature

A	= area, m^2
c	= velocity, m/s
D	= hole diameter, mm
$\boldsymbol{E}, \boldsymbol{F}, \boldsymbol{G}$	= flux vectors
e	= specific total energy, J/kg
H	= cascade height, mm
J	= cell volume, m^3
L	= axial chord length, mm
M	= blowing ratio
Ma	= Mach number
$\dot{m}$	= mass flow, kg/s
p	= pressure, Pa, bar
q	= heat flux, W/m^2
Re	= Reynolds number
s	= coordinate along surface, m
T	= temperature
Tu	= turbulence intensity
t	= spacing, mm
$\boldsymbol{U}$	= vector of conservative variables
u, v, w	= Cartesian velocity components, m/s
x, y, z	= Cartesian coordinates, m
α, β	= flow angles, deg
β_s	= staggering angle, deg
κ	= isentropic exponent
ξ, η, ζ	= arbitrary curvilinear coordinates
ρ	= density, kg/m^3
τ	= component of Reynolds stresses, N/m^2
χ	= coordinate perpendicular to surface

Subscripts

bitan	= bitangential coordinate system
c	= cooling air condition
is	= isentropic
t	= total
1	= at inlet
2	= at exit

Superscript

T	= transposed

Introduction

HIGH-PROCESS efficiencies and high-power-weightratios are two major requirements for the economic operation of both stationary gas turbines and aeroengines. This development leads to extremely high-turbine inlet temperatures and adjusted pressure ratios. The allowable hot-gas temperature is limited by the material temperature of the vanes and blades. Intensive cooling is required to guarantee an economically acceptable lifespan of the components that are in contact with the hot gas. At the present time, the most efficient cooling concept is a combination of convection cooling, impingement cooling, and film cooling. Convection cooling and impingement cooling are based on the admission of cooling air into the interior of the blade through channels. The wall of the hollow blade forms a parting wall between the cooling fluid and the hot exhaust gas. During the flow through the channels, the air takes up the heat from the wall by convection.

A further reduction in the material temperature can be obtained by film cooling. For this purpose, cooling air is injected into the hot gas stream through slots or holes in the blade wall. If designed properly, the cooling air forms an isolating layer on the blade. Reduction of the heat transmission and convection enhances the cooling of the blade surface. Although film cooling has been in use for years[1,2] along the suction side and the pressure side, problems occur in the vicinity of the stagnation point as a result of high stagnation pressures and opposed momentum fluxes. But, in particular, the leading edge must be protected efficiently because thermal load is at its highest in this region. Thus, basic investigations are necessary in this area to achieve a reliable design for cooled blades and vanes. Concerning the computational fluid dynamics research on this subject, a

Received 13 April 1998; revision received 5 October 1998; accepted for publication 16 November 1998.

*Professor, Director of the Institute of Steam and Gas Turbines, Templergraben 55. Member AIAA.
†Research Engineer, Institute of Steam and Gas Turbines, Templergraben 55.
‡Professor, Director of the Institut für Strahlantriebe.
§Research Engineer; currently at MTU München, Germany.

bibliography (1971–1996) of the most important publications can be found in a study by Kercher.[3]

By means of experiments, Beeck[4] investigated a turbine blade cascade with cooling fluid ejection at the leading edge through two slots. His experiments focus mainly on the aerodynamic behavior of the ejection. Thus, the temperature ratio of cooling fluid flow and main flow was equal to unity. Two-dimensional aerodynamic numerical studies of this configuration have been presented by several authors.[5,6] Recent three-dimensional numerical studies of the aerodynamic and thermal behavior of the turbine blade in the case with slot ejection were performed by Bohn et al.[7,8] using a conjugate heat transfer method.[9] Further experimental investigations of the same airfoil geometry, but with shower-head ejection at the leading edge, were performed by Ardey and Fottner.[10,11] In this paper, the results of numerical investigations concerning the two different cooling configurations in the case of a blowing ratio of $M = 1.1$ are presented and compared with the experimental data.[10,11]

Experimental Setup

The experimental investigations were carried out in the High Speed Cascade Wind Tunnel of the University of the Armed Forces Munich[12] on a large-scale high-pressure turbine cascade named AGTB. The cascade consists of three blades, but only the center blade was used for the measurements. The aerodynamic and geometric data of the cascade are listed in Table 1.

Two film-cooling configurations were tested: ejection slots[4] (AGTB-S) and ejection holes[10,11] (AGTB-B1). The ejection angles and locations on the suction side (SS) and on the pressure side (PS) near the stagnation line are identical for both configurations. The slots extend along the entire blade height and have two interceptions (gaps) for the leading-edge retainers. The holes are spread evenly along the entire blade height. The ejection is fed by the plenum inside the blades. The basic AGTB configuration is shown in Fig. 1. The design parameters of the cooling configurations are given in Table 2.

The High Speed Cascade Wind Tunnel operates continuously and isothermally in a large pressurized tank. Thus, the Mach number and Reynolds number can be adjusted independently. The turbulence intensity in the test section can be varied and was set to 5% for the AGTB cascade. The ejected air is supplied by a separate screw compressor that compresses air from the pressure tank and works on the same pressure level as the test facility. A cooler sets the temperature of the secondary air to maintain isothermal conditions. Figure 2 shows the test section of the wind tunnel with the AGTB turbine cascade. Adjustable guide vanes were mounted at the cascade ends to achieve constant inlet pressure distribution. An orifice was set up in the duct of the secondary air for the determination of the coolant mass flow rate. Quartz-glass windows were installed in the front part of the sidewalls to obtain visual access to the leading edge of the center blade.

Table 1 Cascade geometry and parameters

Parameter	Symbol	Value
Chord length	L	250 mm
Cascade height	H	300 mm
Pitch ratio	t/L	0.714
Staggering angle	β_s	73.0 deg
Inlet Mach number	Ma_1	0.37
Inlet Re number	Re_1	3.71×10^4
Inlet flow angle	α_1	47 deg
Inlet turbulence intensity	Tu_1	5%
Isentropic exit Ma number	Ma_{2is}	0.95
Isentropic exit Re number	Re_{2is}	6.95×10^4
Exit flow angle	β_2	28.3 deg

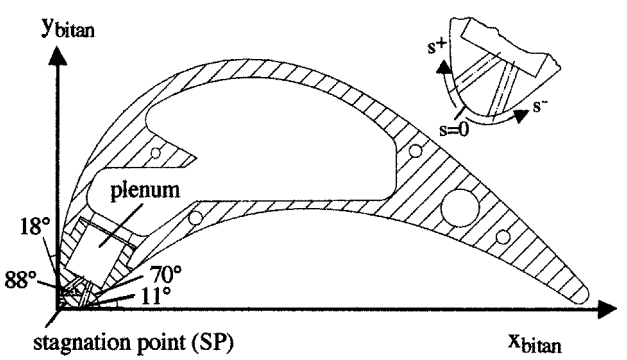

Fig. 1 Blade geometry.

Table 2 Design parameters of cooling configurations

Parameter	Slots	Holes
Position s/L SS	0.02	0.02
Position s/L Ps	−0.03	−0.03
Ejection angle SS	110 deg	110 deg
Ejection angle PS	120 deg	120 deg
Slot width/diameter	2.545 mm	3.00 mm
Slot/hold length	12.5 mm	12.5 mm
Pitch ratio of holes	——	5 ∗ D
Number of holes (row)	——	20

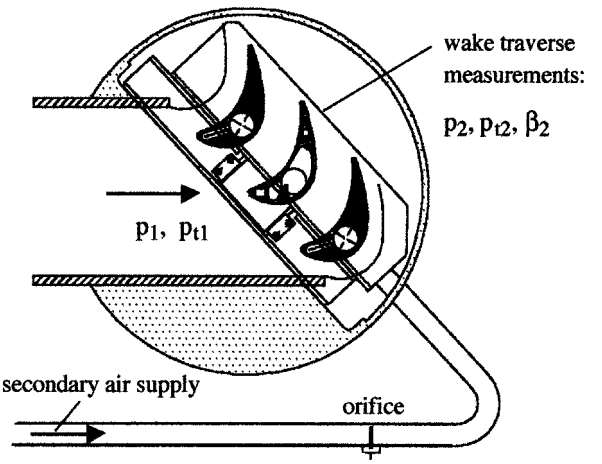

Fig. 2 Test section of the wind tunnel.

The two-dimensional aerodynamic losses were detected 32% of the chord length downstream of the cascade with a wedge probe that was traversed in the midspan section measuring the local values of the static and the total pressures as well as the circumferential flow angles. The secondary flowfield was determined with a five-hole probe being traversed pitchwise and spanwise such as the 32% chord length downstream of the cascade. The loading of the cascade was measured by means of static pressure tappings in the midspan section of the blade. On the AGTB-B1 cascade, an additional number of static pressure tappings were spread close to the holes to gain information about the influence of the ejection jets on the local static pressure distribution. A qualitative study of the ejection fluid propagation on the blade surface was performed using oil-flow visualizations. Schlieren pictures indicated the penetration height of the ejection into the main stream flow, making it possible to choose and adapt the measuring planes for the detailed flowfield investigations that were performed with the laser transit velocimetry and the hot-wire anemometry. The laser transit velocimetry system that was used provides the two-dimensional data of the flow vector in the axial and circumferential directions and the turbulence intensity.[4] The velocity measuring accuracy depends on the turbulence intensity. For the main flow region the error is 3% and for the region of high turbulence level it is 5%. It was employed on the leading edge of the AGTB-S and close to the holes on the AGTB-B1. Farther downstream of the holes of the AGTB-B1, a subminiature triple hot-wire probe was used to determine the three-dimensional flow vectors of the jet trajectory and the components of the Reynolds stress tensor.[13] The velocity measuring error of the three-dimensional hot-wire anemometry is below 3%.

Mathematical Model

The numerical scheme for the simulation of the fluid flow works on the basis of an implicit finite volume method combined with a multiblock technique. The physical domain is divided into separate blocks and the full, compressible, three-dimensional Navier–Stokes equations are solved in the fluid blocks. The governing equations for the conservative variables in arbitrary, body-fitted coordinates ξ, η, and ζ, with the fluxes in normal directions to ξ, η, and ζ = const cell faces, read for the fluid flow:

$$\boldsymbol{U}_t + \boldsymbol{E}_\xi + \boldsymbol{F}_\eta + \boldsymbol{G}_\zeta = \boldsymbol{0} \tag{1}$$

with

$$\boldsymbol{U} = J \cdot (\rho, \rho u, \rho v, \rho w, \rho e)^T \tag{2}$$

$$\boldsymbol{E} = J \cdot (\tilde{\boldsymbol{E}} \cdot \xi_x + \tilde{\boldsymbol{F}} \cdot \xi_y + \tilde{\boldsymbol{G}} \cdot \xi_z) \tag{3}$$

$$\tilde{\boldsymbol{E}} = \begin{bmatrix} \rho u \\ \rho u^2 - \tau_{xx} \\ \rho uv - \tau_{xy} \\ \rho uw - \tau_{xz} \\ (\rho e - \tau_{xx})u - \tau_{xy}v - \tau_{xz}w + q_x \end{bmatrix} \tag{4}$$

$\boldsymbol{F}$ and $\boldsymbol{G}$ are obtained analogously.

The conservation equations are discretized implicitly in the first order in time using Newton's method.[14] Upwind discretization is used for the inviscid fluxes. Godunov-type flux-differencing[15] is employed for the numerical diffusion. To achieve third-order accuracy, van Leer's MUSCL-technique[16] is used. Because this Godunov flux is not sufficiently diffusive to guarantee stability in regions with high gradients, it is combined with a hyperdiffusive modified Steger–Warming flux.[17] The viscous fluxes are approximated using central differences. The resulting system of linear equations is solved by a Gauss–Seidel point iteration scheme allowing high vectorization on present-day computers. The closure of the conservation equations is provided by the algebraic eddy–viscosity turbulence model by Baldwin and Lomax.[18]

Figures 3 and 4 show the computational domains and grids employed for the three-dimensional investigations for one-half of the passage. The grid for the calculation with slots consists of a total of 233,826 grid points, whereas 1,539,807 grid points are necessary for the discretization of the shower-head configuration. The details of Fig. 3 show the discretization of the leading edge, including the plenum and the slots. Because the flow development in the inner geometry significantly influences the flow behavior at the exit of the ejection slots, it is important to include the plenum in the simulations. Symmetry conditions are used in the midspan in both cases. Because the investigated configurations are in a plain cascade, the three-dimensional grid can be obtained by stacking two-dimensional grids in a radial direction, taking the interceptions (gaps) of the slots or the cooling holes, respectively, into account. For the interaction of secondary flows and cooling fluid, the discretization of the half passage including one sidewall is necessary. The details of Fig. 4 show the effort for the discretization of the plenum and the cooling holes. Here, seven radial grid planes are used for every hole, leading to a three-dimensional grid with a total of 153 planes.

Although the numerical effort is extremely high, these grid sizes are of minimum size for this kind of investigation, being focused on sidewall effects and basic ejection-jet phenomena. If one wants to investigate the main flow and ejected flow mixture in detail, the density of the radial planes must be increased distinctly. This means using a numerical effort that is behind the economical use of computational capacities available today. In this case, one has to focus on a blade slice including the holes and using symmetry conditions. Thus, sidewall effects will be neglected in this case.

Total pressure, total temperature, and flow angles at the inlet of the cascade and the plenum inlet are prescribed as boundary conditions (BC) in both cases. The static pressure is fixed at the exit. The inlet profile of the boundary layer is prescribed in accordance with the measurements. The blade is considered fully turbulent. The averaged values of the boundary conditions can be obtained from Table 3. The averaged blowing ratio in both cases is

$$M = (\rho c)_c / (\rho c)_1 = 1.1 \tag{5}$$

Table 3 Boundary conditions

Boundary condition	Slots	Holes
Ma_1 inlet	0.379	0.373
p_{t1} inlet, hPa	201.7	196.5
T_{t1} inlet, K	313	303
p_2 exit, hPa	141.3	145.2
Re_1 inlet	3.71×10^4	3.71×10^4
p_{tc} blow, hPa	229.0	217.1
T_{tc} blow, K	313.0	303.0

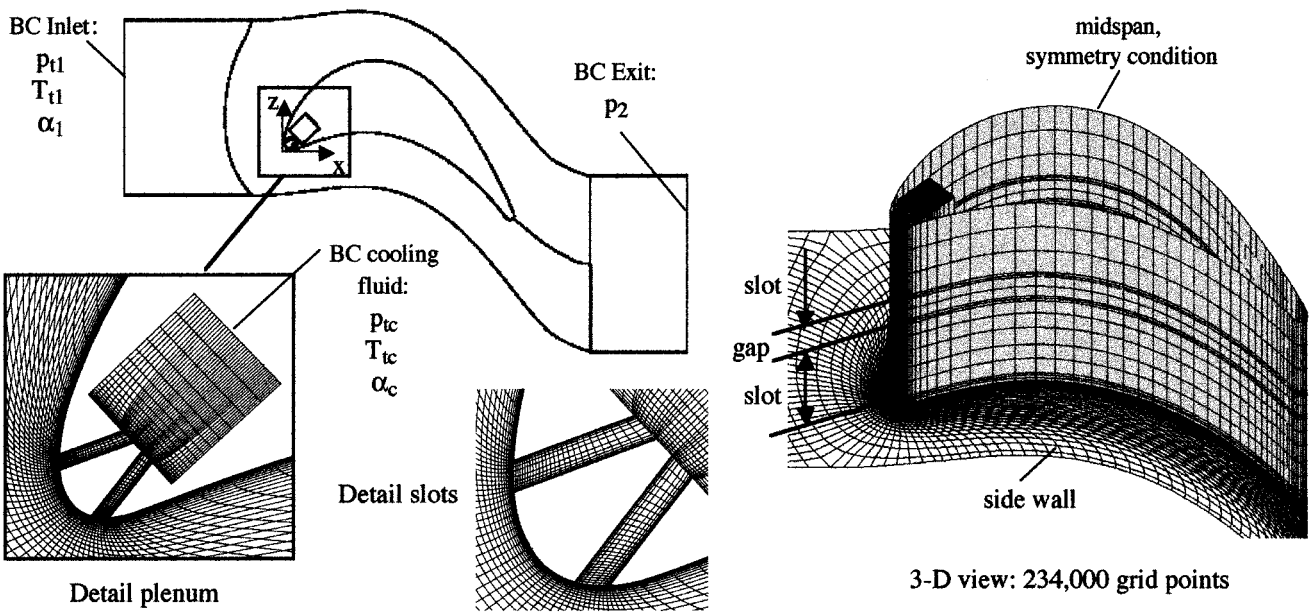

Fig. 3 Computational domain and grid for the configuration with ejection slots.

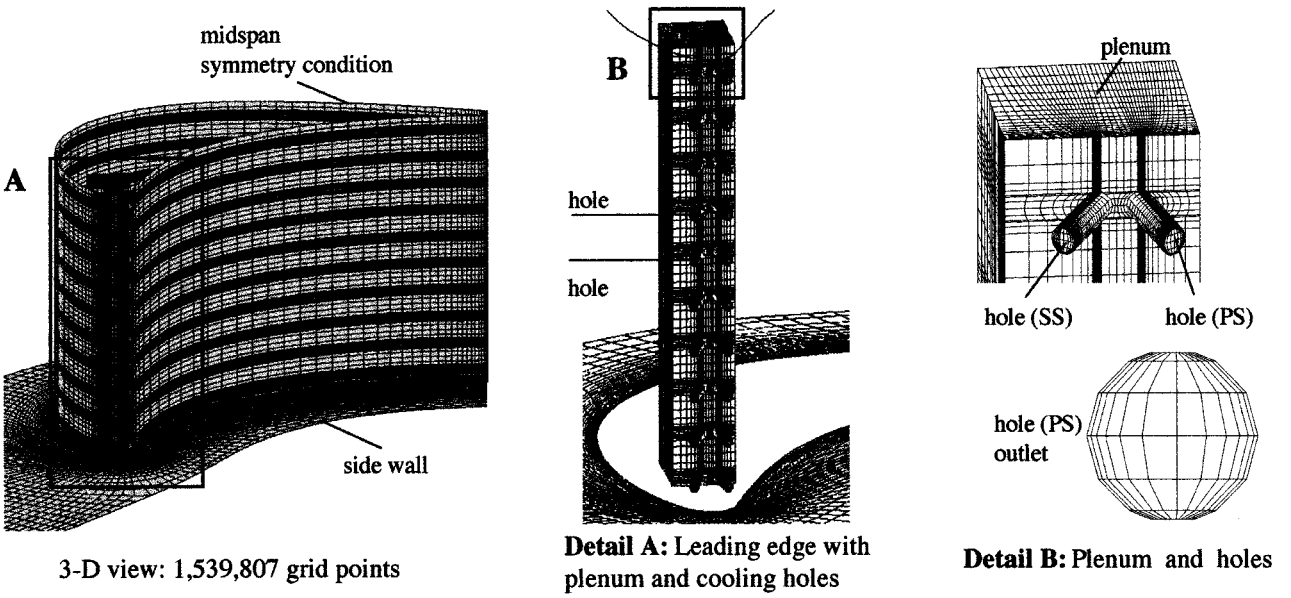

Fig. 4 Computational grid for the configuration with ejection holes.

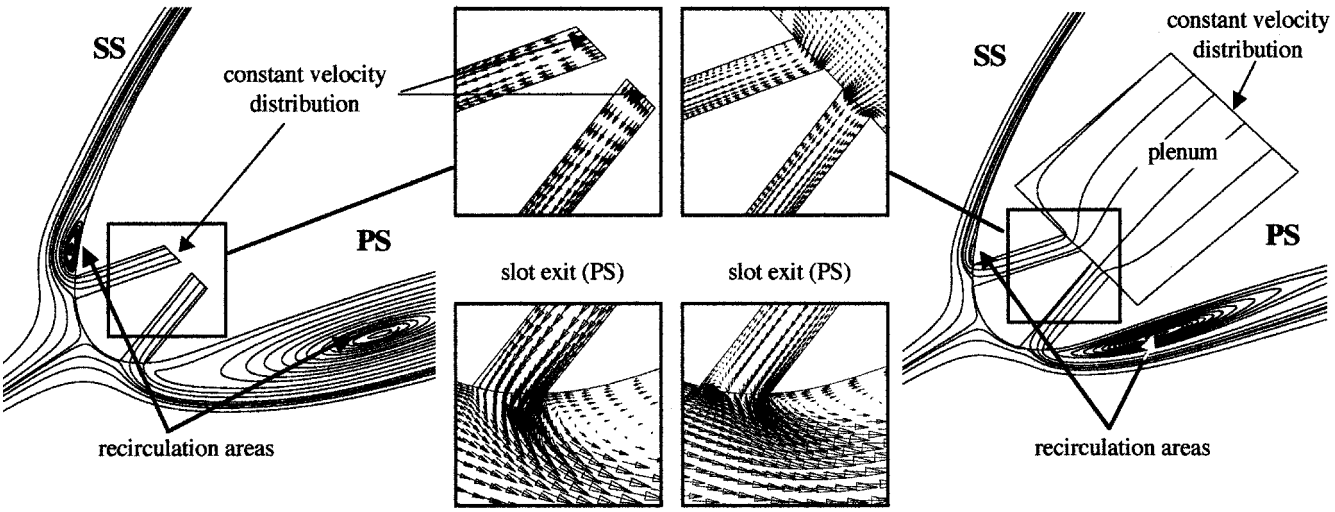

Fig. 5 Influence of interior discretization on the leading-edge flowfield (M = 0.47).

Results

Influence of Plenum Discretization

To evaluate the influence of the plenum discretization, preliminary two-dimensional studies were carried out on the slot ejection with a blowing ratio of $M = 0.47$. Figure 5 gives a comparison of the two-dimensional cases with and without discretization of the plenum. In the first case (left side of Fig. 5), a constant velocity distribution is prescribed at the slot inlets, whereas in the case with plenum discretization, the constant velocity distribution is prescribed at the inlet of the plenum (right side of Fig. 5). This leads to a very inhomogeneous velocity distribution at the slot inlets in the second case. The different velocity distributions at the slot inlets are responsible for significant differences in the calculated aerodynamic behavior of the blade.

The differences in the calculated pressure distributions are shown in Fig. 6a. In particular, the size of a recirculation area on the pressure side downstream of the ejection slot is heavily overestimated in the case without plenum discretization. The correct size of the recirculation areas is known from the laser transit velocimetry measurements.[4] In Fig. 6b, this is underlined by a quantitative comparison of the backflow velocities in both cases. The backflow velocity in the recirculation area and the size of the area is about two times greater than in the case with plenum discretization. In accordance with these results, all further calculations in the three-dimensional cases with slot ejection and shower-head ejection are performed with plenum discretization.

Pressure Distributions

Figure 7a shows a comparison of the experimental and calculated pressure distributions in the midspan of the slot ejection ($M = 1.1$). The numerical results correspond quite well with the experimental data. In the case of the slot ejection, the blowing ratio of $M = 1.1$ leads to large recirculation areas downstream of the slots, particularly on the pressure side. The size of the recirculation area is calculated with good correspondence to the experimental data. In the case of the shower-head ejection (Fig. 7b), the correspondence of the experimental and calculated pressure distribution is excellent on the pressure side and on the rear part of the suction side. On the front part of the suction side, the pressure is calculated slightly higher than the experimental values. That means the sidewall boundary effects in the numerical results have slightly less impact on the flowfield than in the experiment.

Table 4 Experimentally/numerically determined $\dot{m}$ and M

Configuration	$\dot{m}$, 10^{-3} kg s^{-1}	M
Slot ejection	40.08/41.80	1.1/1.14
Shower head	8.34/8.70	1.09/1.11

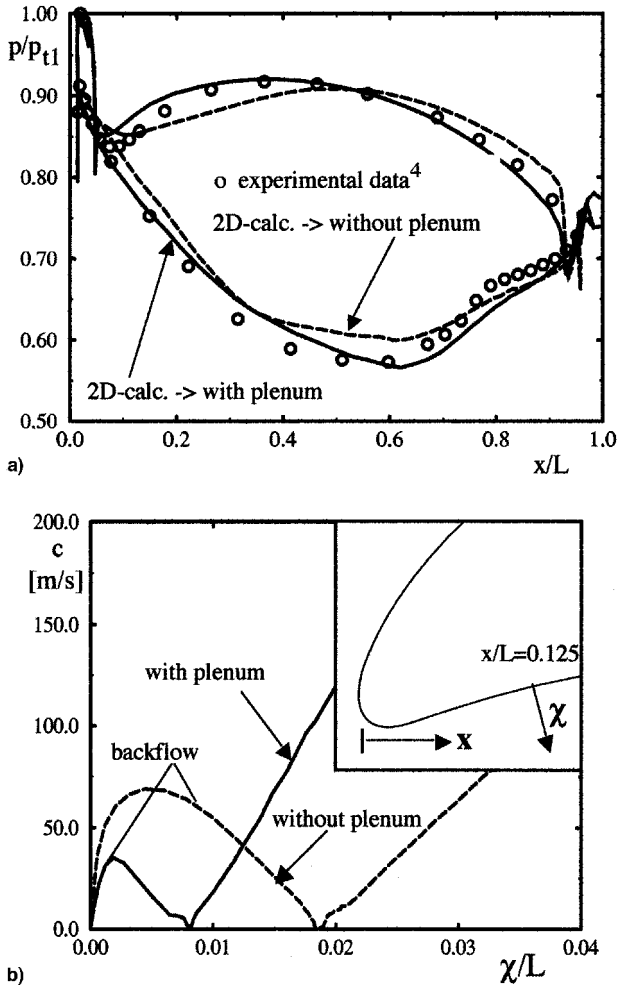

Fig. 6 Influence of interior discretization on the recirculation areas (M = 0.47): a) pressure distribution and b) backflow velocity.

The shower-head ejection leads to smaller recirculation areas downstream of the ejection holes. The different aerodynamic behavior of the blade in the cases of slot ejection and shower-head ejection for the same blowing ratio is caused by the boundary conditions and the alternating cooling path geometry for the configurations. The secondary mass flow in the case of the slot ejection is much higher. Table 4 gives the measured and the calculated cooling mass flows for the different configurations. The numerical values are only slightly higher than in the experiment, although they are a result from the inlet boundary conditions.

Streamline Distributions

Figure 8 shows the distributions of streamlines coming out of the middle of the ejection slots on the pressure and suction sides. A large region on the pressure side is not covered by the ejected fluid (Fig. 8a). This region is much larger than the range of the slot gap, which is free of cooling air ejection. This is a result of the higher static pressure in the height of the gap, because here, the main flow does not have to take the long way around the recirculation area. The region of higher static pressure leads to displacements of the ejected fluid in the direction of the sidewall and the symmetry plane. There also exists a vortex that is generated by fluid circulating through the

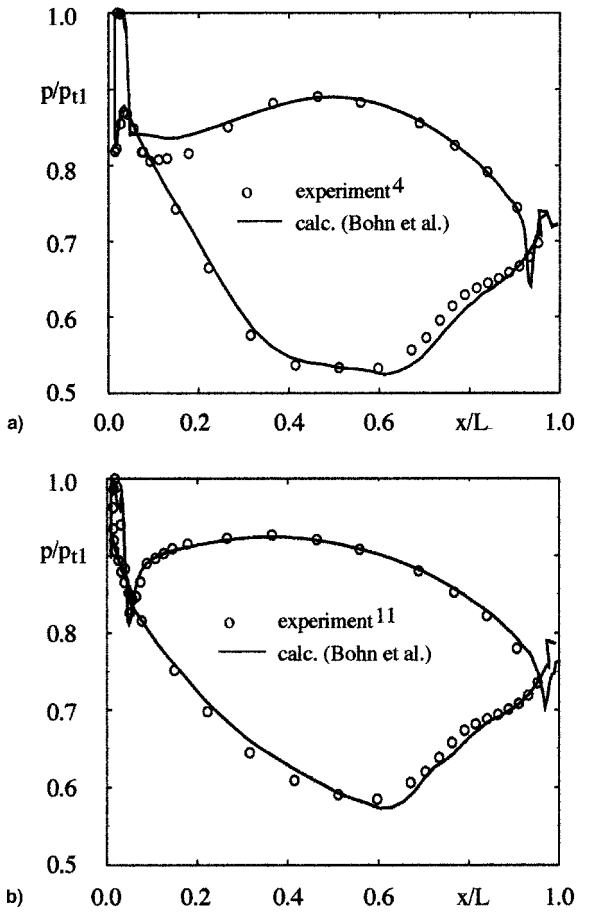

Fig. 7 a) Pressure distribution (slot ejection, M = 1.1) and b) pressure distribution (shower-head, M = 1.1).

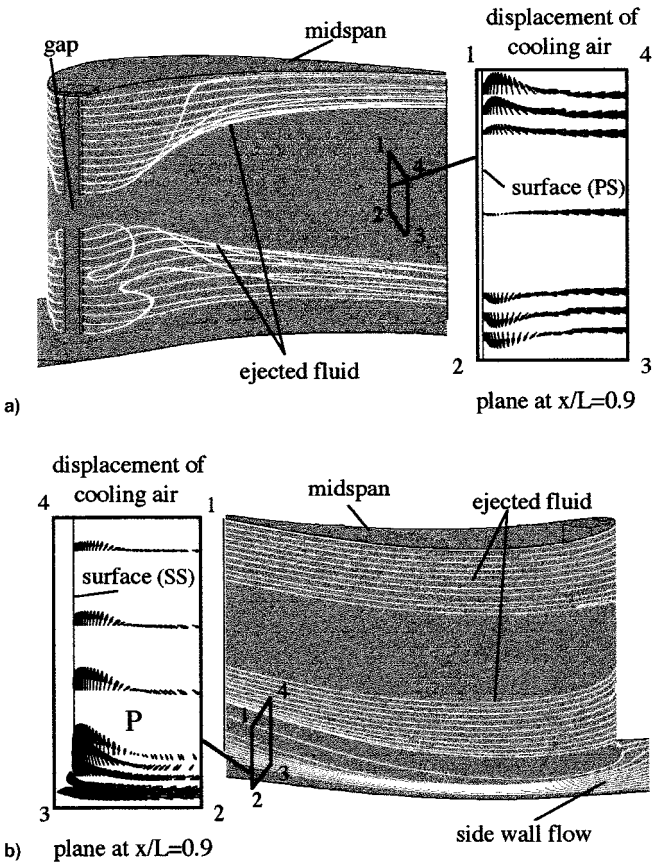

Fig. 8 Ejected fluid distribution (slot ejection, M = 1.1): a) pressure side and b) suction side.

gap area from above the ejected material to the reverse flow region underneath the coolant to fill the deficit of kinetic energy occurring there. This vortex persists throughout the whole blade passage. Therefore, the uncovered region enlarges downstream continuously in the radial direction. The displacement of the ejected fluid on the pressure side is clearly visible using a vector plot (Fig. 8a), which shows the movement of the fluid in the radial direction of a cutting plane perpendicular to the pressure side surface at a position $x/L = 0.9$. Furthermore, the streamline distribution of the cooling fluid in Fig. 8a shows that at the end of the slots, part of the cooling fluid is sucked into the reverse flow region and is lost for cooling purposes.

Focusing on the sidewall of the suction side (Fig. 8b), the streamlines show a displacement of cooling air that is a result of the influence of the passage vortex P on the suction side. The passage vortex is generated in the sidewall boundary layer. The pressure gradient in the passage leads to a greater diversion of the low-momentum fluid in the sidewall boundary layer than of the main flow. Thus, the fluid is conducted toward the suction side. This can be shown by streamlines in the sidewall boundary layer in Fig. 8b. When the fluid reaches the suction side it changes direction and flows toward the midspan, displacing the cooling fluid. The secondary flow vectors of Fig. 8b in a cutting plane perpendicular to the blade at $x/L = 0.9$ show the displacement effect of P on the cooling fluid distribution.

Figure 9 shows the distribution of the cooling fluid on the pressure and suction sides in the case of the shower-head ejection. It becomes obvious that the cooling fluid does not spread out to cover the blade surface after ejection through the holes. Instead of forming a continuous cooling film along the blade surface, separated jets of

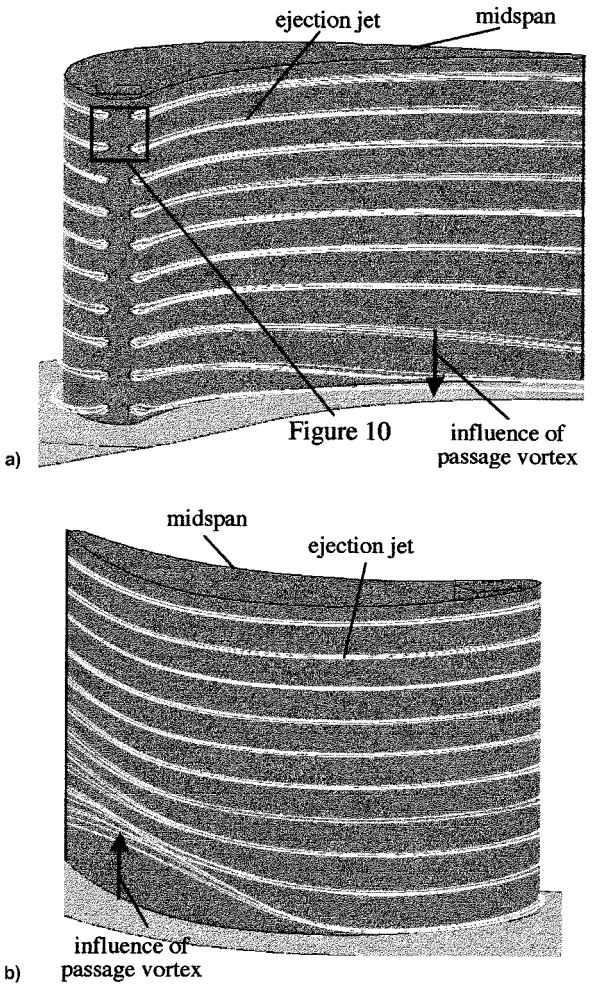

Fig. 9 Ejected fluid distribution (shower-head ejection, M = 1.1): a) pressure side and b) suction side.

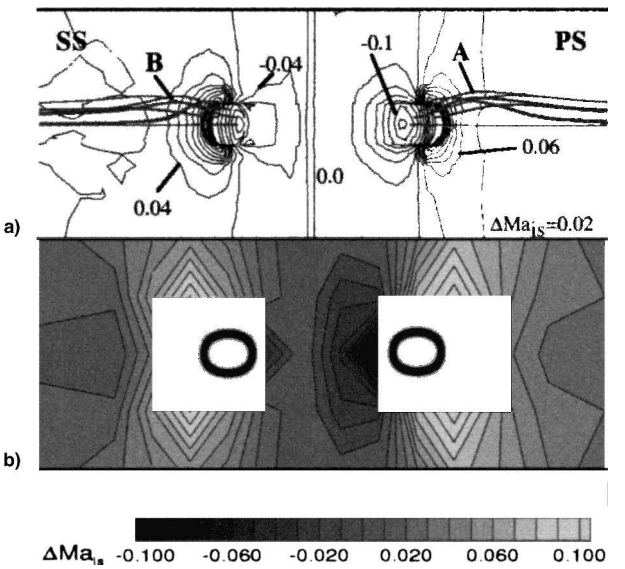

Fig. 10 Leading-edge analysis (shower-head ejection, M = 1.1): a) calculation and b) experiment.

each ejection hole can be found. The reason for this behavior will be shown later by an investigation on the secondary flows in the jets.

The isolated jets are distributed evenly on the pressure side. A slight displacement effect by the passage vortex can be detected for the three jets near the sidewall (Fig. 9a). On the suction side, the displacement of the ejected fluid near the sidewall in the direction of the midspan can be detected analogously to the slot configuration. The effect is at least as strong as in the case of the slot ejection. The influence of the passage vortex is obvious (Fig. 9b) for five ejection jets near the sidewall.

Figure 10 gives a detailed view on the ejection zone at the leading edge. On the pressure side, the cooling fluid attempts spreading out (streamtubes, A), but then it is forced back and forms one distinct jet. The same effect can be found on the suction side (streamtubes, B). The isolines on the surface (Fig. 10a) give the differences between the isentropic Mach number distributions of the calculation with ejection and a reference calculation without ejection. The isentropic Mach number is defined:

$$Ma_{is} = \sqrt{\left\{2/(\kappa - 1) \cdot \left[(p_{t1}/p)^{(\kappa-1)/\kappa} - 1\right]\right\}} \qquad (6)$$

In front of the hole exits, in particular on the pressure side, main flow stagnation in front of the jets is obvious, whereas the low static pressure in the recirculation areas (jet wakes) is leading to higher isentropic Mach number values than in the calculation without ejection. The main stream flow is displaced by the cooling fluid that forms an obstacle at the exit of the cooling holes. The effective cross section for the main stream flow is diminished, and therefore, it is being accelerated in between the cooling jets leading locally to a lowered static pressure. When the main stream flow and the cooling fluid have reached the same flow direction, the obstacle effect has almost disappeared, so that it can no longer be detected by static pressure means. The static surface probe measurements (Fig. 10b) in the leading-edge region reveal the same effects and are in good correspondence with the numerical results.

Secondary Flows in the Jets

In the case of the shower-head ejection, the streamline visualization has shown that the ejected cooling fluid forms distinct jets along the surfaces, instead of a continuous cooling film. Therefore, regions between these cooling jets exist that are not sufficiently covered by the cooling fluid. The reason for this behavior can be determined by the experimental measurement and numerical investigation of secondary flow vectors in the cooling jets. Figure 11 shows the positions of the experimental investigation planes of the three-dimensional

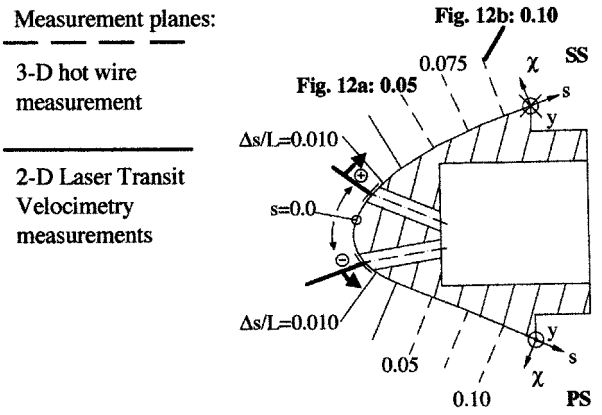

Fig. 11 Experimental measurement planes.

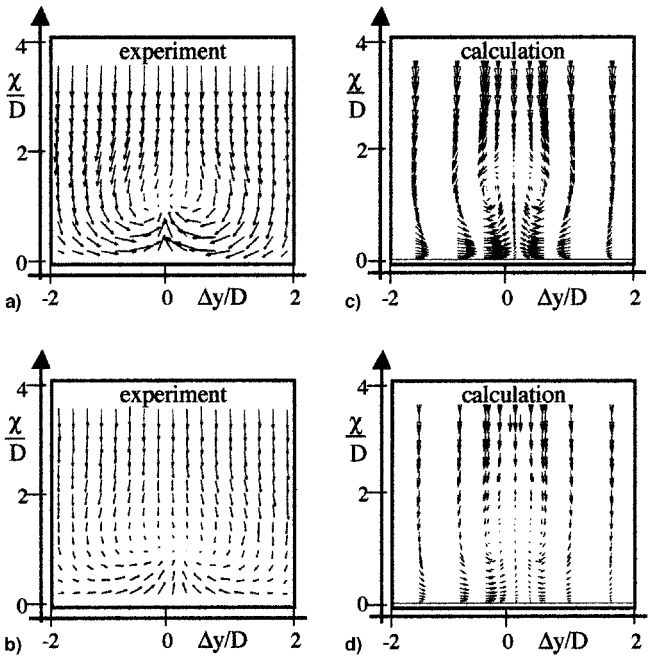

Fig. 12 Development of kidney vortex in ejection jet (SS, M = 1.1). $\Delta s/L$ = a) 0.05, b) 0.10, c) 0.05, and d) 0.10.

hot-wire measurements and the laser two-dimensional velocimetry measurements. In Fig. 12, these results are displayed in an exemplary manner for two different cutting plane positions (indicated in Fig. 11) on the suction side in comparison with the calculational results. The direction of χ / D is perpendicular to the blade wall. The position $\Delta y / D = 0$ marks the height of the centerline of the hole. The vector plots reveal the existence of kidney vortices that have stabilizing effects on the cooling fluid jets along the blade surface. Both results show that the cores of the kidney vortices can be found at a distance of about one diameter of a cooling hole away from the blade surface. The cores only slightly change their positions in the investigated planes.

The kidney vortex is created through the interaction of ejected fluid and main stream flow. In the shear layer of ejected fluid and main stream, the ejected fluid is deflected toward the main stream direction. The deflected fluid cannot penetrate into the cooling jet that maintains its original direction. Therefore, the cooling fluid in the shear layer is not only deflected toward the main stream direction, but also turns sideways, forming the vortex. By creating the vortex in its shear layer, the cooling jet turns gradually toward the main stream direction.

Conclusions

Extensive experimental and numerical investigations have been carried out to research the interactions of main stream and ejected fluid in turbine blade cascades with leading ejection through slots and holes. For numerical studies, it is necessary to include the plenum or the internal cooling channel in the calculation, because otherwise, the aerodynamics of the ejected fluid will be calculated with a significant error. The reasons are the complex velocity distributions at the inlets of the slots and holes and total pressure losses at the inlets. The interaction of the passage vortex with the ejected fluid is of major interest in the design of such cooling configurations. These sidewall effects will lead to a displacement of cooling fluid on the suction side, leaving a large region uncovered with cooling fluid. In the case of the slot ejection, interceptions of the slots must be prevented, otherwise a large area behind the interception will not be covered by the ejected fluid. Shear-layer effects lead to the development of kidney vortices in the jets in the case of the hole ejection. These vortices prevent the ejected fluid from spreading out along the surface. Instead of this, single fluid jets are formed, leaving surface regions uncovered between the jets.

Acknowledgments

The measurements on the AGTB-S cascade were performed within the scope of a project funded by the German Bundesministerium der Verteidigung (German Ministry of Defence). The measurements on the AGTB-B1 cascade were performed within the scope of a project of the German research cooperation on high-temperature gas turbines (AG Turbo), which was funded by the German Ministry of Education, Science, Research, and Technology (BMBF); the Motorenund Turbinen Union München; and the Siemens AG. Permission for the publication of the results is gratefully acknowledged.

References

[1]Schönung, B., and Rodi, W., "Prediction of Film-Cooling by a Row of Holes with a Two-Dimensional Boundary-Layer Procedure," *Journal of Turbomachinery*, Vol. 109, Oct. 1987, pp. 579–587.

[2]Bassi, F., Rebay, S., Savini, M., Colantuoni, S., and Santoriello, G., "A Navier–Stokes Solver with Different Turbulence Models Applied to Film-Cooled Turbine Cascades," *Proceedings of the Advisory Group for Aerospace Research & Development (AGARD) Meeting on Heat Transfer and Cooling in Gas Turbines*, 1992 (CP-527-41).

[3]Kercher, D. M., "A Film-Cooling CFD Bibliography: 1971–1996," *International Journal of Rotating Machinery*, Vol. 4, No. 1, 1998, pp. 61–72.

[4]Beeck, A., "Strömungsfelduntersuchungen zum aerodynamischen Verhalten eines hochbelasteten Turbinengitters mit Kühlluftausblasung an der Vorderkante," Ph.D. Dissertation, Univ. of the Armed Forces Munich, Germany, 1992.

[5]Beeck, A., Fottner, L., Benz, E., and Wittig, S., "The Aerodynamic Effects of Coolant Ejection in the Leading Edge Region of a Film-Cooled Turbine Blade," *Proceedings of the Advisory Group for Aerospace Research & Development (AGARD) Meeting on Heat Transfer and Cooling in Gas Turbines*, 1992 (CP-527-35).

[6]Irmisch, S., "Simulation of Film-Cooling Aerodynamics with a 2D Navier–Stokes Solver Using Unstructured Meshes," American Society of Mechanical Engineers, Paper 95-GT-24, June 1995.

[7]Bohn, D., Kusterer, K., and Schönenborn, H., "3-D Numerical Simulation of the Flow Through a Turbine Blade Cascade with Cooling Injection at the Leading Edge," American Society of Mechanical Engineers, Paper 96-GT-150, June 1996.

[8]Bohn, D., Becker, V., and Kusterer, K., "3-D Conjugate Flow and Heat Transfer Calculations of a Film-Cooled Turbine Guide Vane at Different Operating Conditions," American Society of Mechanical Engineers, Paper 97-GT-23, June 1997.

[9]Bohn, D., Schönenborn, H., Bonhoff, B., and Wilhelmi, H., "Prediction of the Film-Cooling Effectiveness in Gas Turbine Blades Using a Numerical Model for the Coupled Simulation of Fluid Flow and Diabatic Walls," *Proceedings of the International Symposium on Air Breathing Engines*, Sept. 1995 (Paper 95-7105).

[10]Ardey, S., and Fottner, L., "Flow Field Measurements on a Large Scale Turbine Cascade with Leading Edge Film Cooling by Two Rows of Holes," American Society of Mechanical Engineers, Paper 97-GT-524, June 1997.

[11]Ardey, S., and Fottner, L., "Untersuchungen am Turbinengitter AGTB-B1 mit Vorderkanten-Kühlluftausblasung zur Bestimmung des Gitterverhaltens bei Variation der Ausblaserate," Univ. of the Armed Forces Munich, Inst. für Strahlantriebe, Rept. LRT-WE12-96/02, Jan. 1996.

[12]Sturm, W., and Fottner, L., "The High Speed Cascade Wind Tunnel of the German Armed Forces University Munich," *Proceedings of the 8th*

Symposium on Measuring Techniques for Transonic and Supersonic Flows in Cascades and Turbomachines, Genoa, Italy, 1985.

[13]Wunderwald, D., Wilfert, G., and Fottner, L., "The Experimental Set-Up of a Triple-Sensor Anemometry and Its Controlling System at the High-Speed Cascade Wind Tunnel," *Proceedings of the 11th Symposium on Measuring Techniques for Transonic and Supersonic Flows in Cascades and Turbomachines*, edited by L. Fottmer, Inst. für Strahlantriebe, Univ. of the Armed Forces Munich, Germany, 1992.

[14]Schmatz, M. A., "Three-Dimensional Viscous Flow Simulations Using an Implicit Relaxation Scheme," *Notes on Numerical Fluid-Mechanics (NNFM)*, Vol. 22, Vieweg, Brunswick, Germany, 1988, pp. 226–242.

[15]Eberle, A., "Characteristic Flux Averaging Approach to the Solution of Euler's Equations," *Lecture Series 4 'Computational Fluid Dynamics at VKI, Part I and II*,' von Kármán Inst. for Fluid Dynamics, Rhode Saint Genèse, March 1987.

[16]Anderson, W. K., Thomas, J. L., and Van Leer, B., "A Comparison of Finite Volume Flux Vector Splittings for the Euler Equations," AIAA Paper 85-0122, Jan. 1985.

[17]Eberle, A., Schmatz, M. A., and Bissinger, N., "Generalized Flux vectors for Hypersonic Shock-Capturing," AIAA Paper 90-0390, Jan. 1990.

[18]Baldwin, B. S., and Lomax, H., "Thin Layer Approximation and Algebraic Model for Separated Turbulent Flows," AIAA Paper 78-257, Jan. 1978.